ACS APPLIED MATERIALS & INTERFACES

Research Article

www.acsami.org

Nanosheets Co_3O_4 Interleaved with Graphene for Highly Efficient Oxygen Reduction

Taiwo Odedairo,[†] Xuecheng Yan,[‡] Jun Ma,[§] Yalong Jiao,[∥] Xiangdong Yao,[‡] Aijun Du,[∥] and Zhonghua Zhu*[,†]

[†]School of Chemical Engineering, The University of Queensland, St. Lucia, Brisbane, Queensland 4072, Australia

[‡]Queensland Micro- and Nanotechnology Centre, Griffith University, Nathan Campus, Nathan, Queensland 4111, Australia

[§]School of Engineering, University of South Australia, Mawson Lakes, South Australia 5095, Australia

[∥]School of Chemistry, Physics and Mechanical Engineering, Queensland University of Technology, Brisbane, Queensland, 4000, Australia

Supporting Information

ABSTRACT: Efficient yet inexpensive electrocatalysts for oxygen reduction reaction (ORR) are an essential component of renewable energy devices, such as fuel cells and metal-air batteries. We herein interleaved novel Co_3O_4 nanosheets with graphene to develop a first ever sheet-on-sheet heterostructured electrocatalyst for ORR, whose electrocatalytic activity outperformed the state-of-the-art commercial Pt/C with exceptional durability in alkaline solution. The composite demonstrates the highest activity of all the nonprecious metal electrocatalysts, such as those derived from Co_3O_4 nanoparticle/nitrogen-doped graphene hybrids and carbon nanotube/nanoparticle composites. Density functional theory (DFT) calculations indicated that the outstanding performance originated from the significant charge transfer from graphene to Co_3O_4 nanosheets promoting the electron transport through the whole structure. Theoretical calculations revealed that the enhanced stability can be ascribed to the strong interaction generated between both types of sheets.

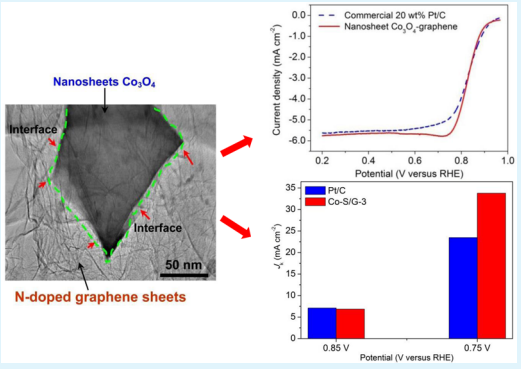

KEYWORDS: *Nanosheets Co_3O_4, sheet-on-sheet heterostructure, fuel cell, nonprecious metal, oxygen reduction reaction*

INTRODUCTION

The looming energy crisis has trigged extensive research into the development of various types of sustainable energy conversion and storage systems.[1] Oxygen reduction reaction (ORR) is a key process for energy conversion and storage in fuel cells, metal-air batteries as well as other applications including water purification, oxygen detection and corrosion protection.[2,3] A major limiting factor of energy-conversion efficiency for current fuel cells is the sluggish kinetics of ORR at the cathode.[4] Platinum (Pt)-based materials are the most efficient electrocatalysts, but their use in large-scale commercial applications is limited due to high cost, poor durability, and scarcity.[5,6] Although low-cost, nonprecious metal electrocatalysts[7,8] have been developed as potential replacement to Pt, two formidable challenges remain including inferior ORR to Pt/C catalysts[9] and unsatisfactory stability and durability.

Of all carbon materials, graphene is the most promising for accommodating various nanoparticles to achieve high electron transport rate, electrolyte contact area and structural stability,[10,11] all of which lead to markedly improved ORR performance. Graphene composites containing Co_3O_4 nanoparticles have shown remarkable ORR performance and thus they are recognized as a class of highly effective, nonprecious electrocatalysts.[4] Prompted by these unique properties, many Co_3O_4 nanostructures, including nanocubes/boxes, nanowires, nanowalls, nanotubes and ordered mesoporous structures have been synthesized and investigated.[12−14] By contrast, Co_3O_4 nanosheets (Co−S) have rarely been reported let alone their ORR performance—nanosheets generally have far more surface area than nanoparticles, thus providing more reactive sites between the electrode and the fuel. A well-known limitation of nanosheets is that they stack unless proper surface functionalizations[15,16] or purpose-designed carriers or spacers are made.[17] A hypothesis made herein was that Co−S spaced by graphene sheets would provide sufficient reactive sites with interconnected channels for electrolyte and thus should show highly improved ORR performance. In our opinion, two prerequisites for a high-performance Co_3O_4 nanosheet/graphene composite (denoted as Co−S/G) include (1) Co−S should not only interleave but also form strong bonding with graphene sheets, which can enhance electrical conductivity and electrochemical properties,[18] and (2) the robust 3D hetero-

Received: July 6, 2015
Accepted: September 8, 2015
Published: September 8, 2015

DOI: 10.1021/acsami.5b06063
ACS Appl. Mater. Interfaces 2015, 7, 21373−21380

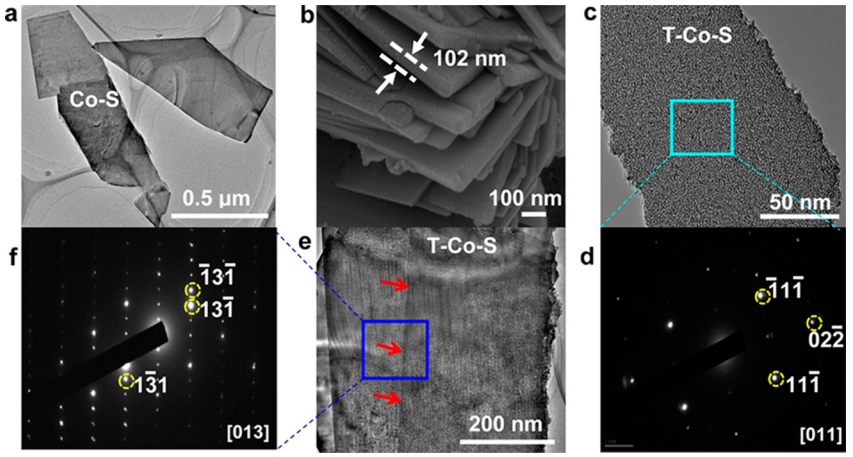

Figure 1. TEM and FESEM micrographs of the Co−S and T−Co−S. (a) TEM of cobalt nanosheets (denoted Co−S). (b) FE-SEM of plasma-treated cobalt nanosheets (T−Co−S). (c) TEM of T−Co−S. (d) Selected area electron diffraction (SAED) pattern [011] fcc of T−Co−S in (c). (e) TEM of T−Co−S, and (f) SAED pattern [013] fcc of T−Co−S in panel e, indicating the existence of a layered structure (superstructure).

structure of Co−S/G is essential to prevent structural collapse and/or catalysts detachment which often occurred for many carbon-supported metal catalysts.[19]

Herein, we report novel approaches for the fabrication of Co_3O_4 nanosheets and for the development of a novel 3D sheet-on-sheet heterostructured Co−S/G. The microwave argon-plasma synthesis approach we adopt in this study not only reduces graphene oxide but effectively disperses Co_3O_4 nanosheets among the graphene sheets. Of all the nonprecious metal electrocatalysts, Co−S/G demonstrates the highest electrocatalytic activity for ORR in alkaline medium. It exhibits superior ORR performance to the commercial state-of-the-art 20 wt % Pt/C (hereafter abbreviated as Pt/C; Vulcan XC-72) with exceptional durability. Density functional theory (DFT) calculations indicate that the unusual electrocatalytic properties of Co−S/G are originated from the significant charge transfer from graphene to Co_3O_4 nanosheets, which would significantly enhance the electron transport throughout the whole structure. Theoretical calculations also reveal that the superior stability of Co−S/G is due to the high interfacial binding energy between graphene and Co_3O_4 nanosheets. Interleaving materials with analogous morphology such as our Co−S/G represents a new class of efficient, robust, and economic ORR electrocatalyst which hold promise to replace the Pt-based catalysts for electrochemical conversions.

MATERIALS AND METHODS

Material Synthesis. Co−S was synthesized via a simple urea based approach. First, 10 mL of $Co(NO_3)_2{\cdot}6H_2O$ (0.055 mol/L) solution was added to 25 mL ethanol at room temperature. This was followed by the dropwise addition of 50 mL of NH_2CONH_2 (0.033 mol/L) used as a structure directing agent under continuous stirring over a period of 3 h at room temperature. The slurry was then transferred into an autoclave for hydrothermal reaction at 120 °C for 28 h. The precipitates were filtered, washed with deionized water and absolute ethanol 3 times and left to dry overnight at 40 °C. The Co−S treated by microwave argon-plasma (750 W, 5 s) is denoted as T−Co−S.

Co−S/G was synthesized by a two-step method. In the first step, Co−S was mixed with graphene oxide (GO) slurry (60 wt % GO in water) prepared by a modified Hummer's method to produce three mixtures where the ratios of Co−S to the slurry remain respectively at 1:6, 1:3, and 2:3; each mixture was sonicated for 1 h and then mixed by a magnetic stirrer for another 2 h at room temperature, followed by a drying process at 40 °C. Second, microwave-plasma exfoliation reactions were performed in a microwave reactor (SAIREM) in conjunction with a vacuum system (~10^{-2} Torr). To produce Co−S/G, we placed in the microwave plasma system and pumped down for 30 min 500 mg of dried GO-cobalt nanosheets in the presence of argon gas (10 cc/min). Once the microwave power was increased to 750 W, the dried GO-cobalt nanosheets were treated for 5 s, resulting in a volume-expansion ratio of around 75 times; this creates expanded products (Co−S/G). The final products with varying ratios of T−Co−S to G (1:6, 1:10, and 1:23) are denoted as Co−S/G-1, Co−S/G-2, and Co−S/G-3, respectively (Table S1, Figures S1 and S2). All the composites were doped with nitrogen by thermally annealing in ammonia at 500 °C for 3 h with a heating rate of 5 °C/min. As a benchmark, Co_3O_4 nanoparticle/graphene composite (Co−P/G) was also synthesized.

Sample Characterization. The material morphology was examined by a field emission scanning electron microscope (FE-SEM, JEOL JSM 7100F) and a high resolution transmission electron microscope (HRTEM, JEOL 2100) operating at 200 kV. X-ray photoelectron spectroscopy (XPS) spectra were acquired on a Kratos Axis ULTRA X-ray photoelectron spectrometer. The binding energies were determined using the C 1s line at 284.6 eV from adventitious carbon as a reference. Recorded spectra were fitted using Gaussian−Lorentzian curves in order to determine the binding energies of the different element core levels more accurately. The Co content was determined by inductively coupled plasma optical emission spectrometry (ICP-OES, Varian 720-ES). Raman spectra were collected with a Renishaw inVia Raman spectrometer equipped with a Leica DMLM microscope and a 514 nm Ar^+ ion laser as an excitation source. Phase purity of the catalysts was determined by X-ray diffraction in a Bruker Advanced X-ray diffractometer using nickel-filtered Cu Kα X-ray source radiation. The N_2 adsorption measurements of the calcined samples were performed using a Tristar II 3020.

Electrochemical Characterization. Rotating disk electrode (RDE) and Rotating ring-disk electrode (RRDE) measurements were performed using a CHI Electrochemical Station (Model 760E) in a standard three-electrode cell. A 4.0 mm diameter glassy carbon disk (disk geometric area 0.126 cm^2) was used as the working electrode; a Pt wire and Ag/AgCl (in saturated KCl solution) were used as the counter and reference electrodes, respectively. Before use, the electrode was polished to mirror flat with alumina powder. The ink formulation (Co−S/G, Co−P/G, or 20 wt % Pt on Vulcan XC-72, Premetek) is 1 mg of catalyst in a 2.3:1 water−ethanol mixture (1 mL) containing 20 μL of Nafion solution (5 wt %). The ink was shaken and sonicated in a bath sonicator for 1 h, and 10 μL of catalyst ink was loaded on the electrode surface resulting in a catalyst loading of ~0.08 mg/cm^2. Prior to testing, the electrolyte of 0.1 M KOH was saturated with O_2 for at least 30 min, and O_2 purging was kept during electrochemical experiments. See the Supporting Information for further details.

DOI: 10.1021/acsami.5b06063
ACS Appl. Mater. Interfaces 2015, 7, 21373−21380

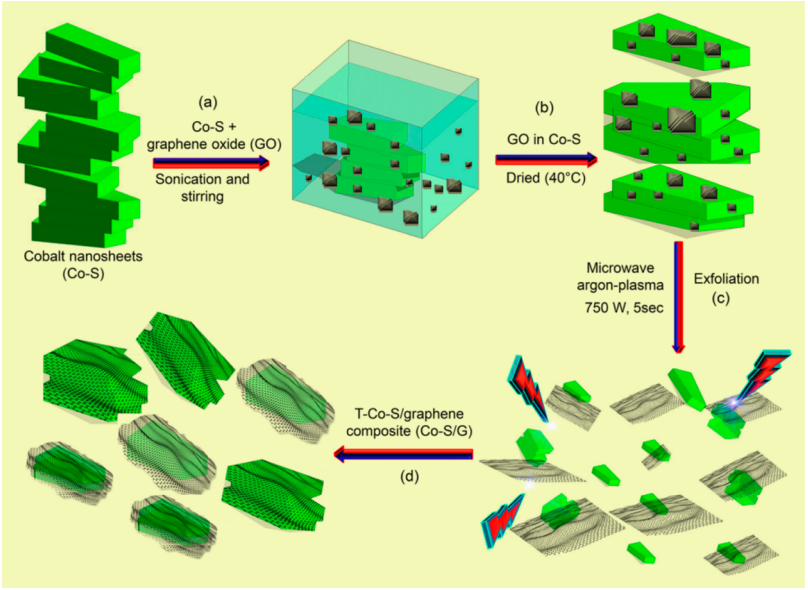

Figure 2. Scheme for fabrication of Co−S/G composites. (a) Sonication and stirring of Co−S with graphene oxide (GO). (b) Formation of GO in Co−S. (c) Exfoliation of GO in Co−S under microwave argon-plasma, where GO was reduced. (d) Formation of T−Co−S/graphene composites (Co−S/G).

RESULTS AND DISCUSSION

Morphology of Sample. Transmission electron microscopy (TEM) image of as-obtained Co_3O_4 nanosheets (Co−S) precursor shows a sheet-like morphology with a lateral dimension of 1−10 μm (Figure 1a). Field-emission scanning electron microscopy (FESEM) reveals that the thickness of a representative sheet is ∼100 nm (Figure 1b). The treated Co−S precursor (T−Co−S) is actually nanosheets constructed from numerous nanocrystals with small intercrystallites (Figure 1c), and the selected area electron diffraction (SAED) pattern (Figure 1d) suggests the degree of orientation with a face-centered cubic structure. Figure 1e contains TEM micrograph of a few-layer T−Co−S, where lines indicated by red arrows may correspond to stacked structure; the SAED pattern (Figure 1f) reveals each weak intensity diffraction spot between strong intensity spots, and this refers to the formation of a layered T−Co−S structure (superstructured).[20,21] The crystallographic structure of T−Co−S is analyzed by X-ray powder diffraction (XRD) as shown in Figure S3; the diffraction peaks can be indexed to cubic phase Co_3O_4 (JCPDS no. 42−1467).

Nanosheets naturally stack themselves together due to high surface area severely disadvantaging their applications. An effective solution is to use macromolecules to prevent stacking, known as exfoliation in polymeric matrices.[22,23] We herein exfoliated Co_3O_4 nanosheets (Co−S) in the matrix of graphene oxide (GO) that features a high density of oxygen functional groups including carboxylic, hydroxyl, and epoxy groups.[15] Because both Co−S and GO are rich in oxygen, they should interact with each other. Figure 2 illustrates the overall synthesis approach for Co−S/graphene (Co−S/G) composites, which was conducted in a microwave-plasma system. The mixture of Co−S and GO slurry was first sonicated and stirred for 3 h, followed by drying. The dried powder was exfoliated under microwave argon-plasma (750 W, 5 s) to produce Co−S/G composites. The morphologies and microstructure of reduced graphene oxide (G) and their composites were investigated as below.

An FESEM image (Figure S4a, Supporting Information) reveals that the reduced graphene oxide (G) produced via the microwave argon-plasma approach possesses 3-D interconnected framework with randomly open macroporous structure ranging from a few hundred nanometers to several microns. A TEM image of G sheets reveals flexible, wrinkled few-layer structure, while its SAED pattern matches well with those of 2−3 layered graphene structure (Figure S4b, Supporting Information). Figure 3a−g and Figure S5 show microstructure of the Co−S/G composites. T−Co−S and graphene sheets are obviously interleaved, implying more or less interactions between T−Co−S and G. The surface functional groups of G provide nucleation sites for the nanosheets, thus resulting in an interleaved morphology. Figure 3a−d reveals the HRTEM images of Co−S/G-3, showing a seemingly strong interaction between the T−Co−S and the G; the SAED pattern in Figure 3e confirms the presence of cubic lattice structure of Co_3O_4 nanosheets.[24] In Figure 3f, the layered structure of Co_3O_4 nanosheets (marked by arrows) is more evident in the composite (Co−S/G-2), while the SAED pattern reveals the lattice structure of Co_3O_4 (Figure S5d).

XRD, Raman, and XPS Studies. The composite XRD patterns show that the (002) diffraction for 0.34 nm intergraphene spacing is hardly visible; indicating the likely uniform dispersion of few-layer graphene sheets (Figure 3h). The obvious increase in the low-angle diffraction means the presence of high density of pores,[25] which agrees well with the nitrogen adsorption−desorption measurements (Figure S1). The Co_3O_4 sheet/graphene composites (Co−S/G-2 and Co−S/G-3) reveal traces of Co_3O_4; by contrast, pronounced peak intensities of Co_3O_4 is observed in nanoparticle/graphene composite (Co−P/G). This might suggest that most Co−S would be sandwiched with graphene sheets in Co−S/G-2 and Co−S/G-3, while Co_3O_4 nanoparticles would stay on the sheet surface in Co−P/G.

The samples Raman spectra show two prominent peaks at 1354 and 1594 cm^{-1}, which correspond to the D and G bands of graphene (Figure S6). Other Raman peaks observed at 464

DOI: 10.1021/acsami.5b06063
ACS Appl. Mater. Interfaces 2015, 7, 21373−21380

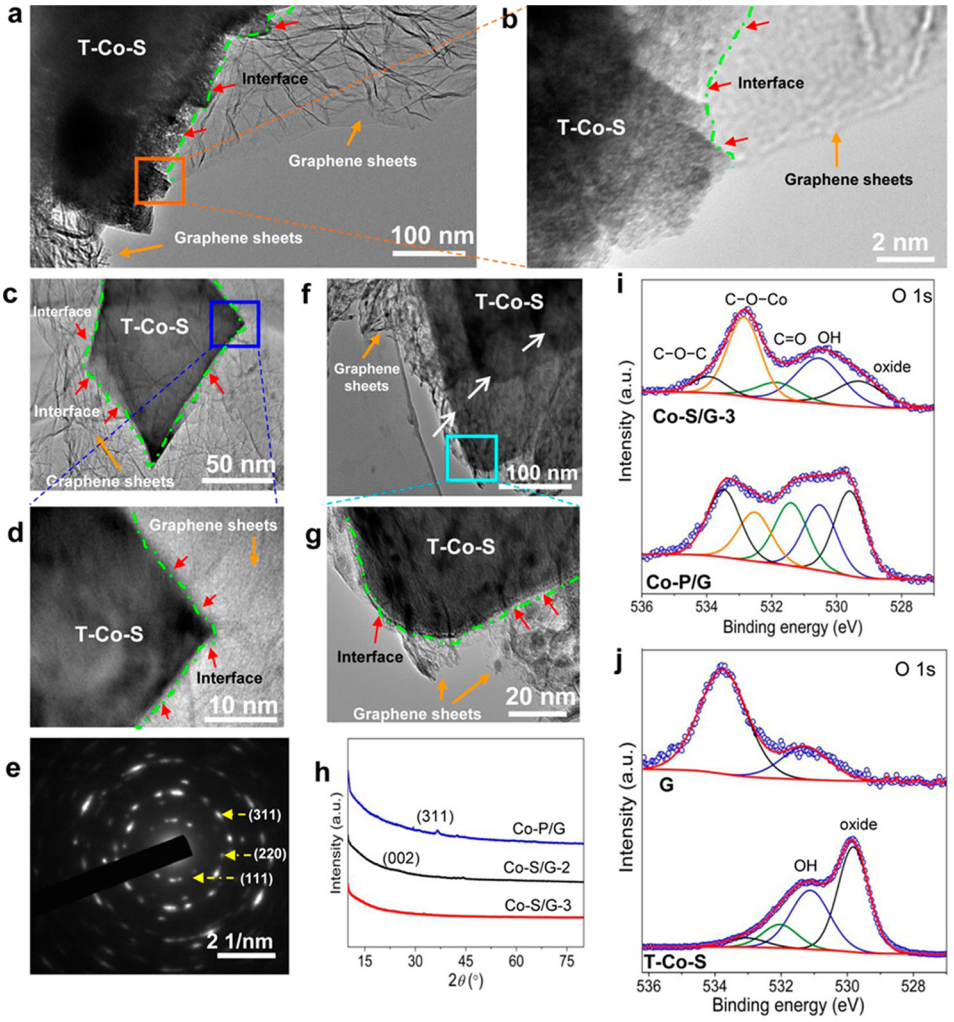

Figure 3. Structural and compositional characterization of Co_3O_4 sheet/graphene (Co–S/G) composites. (a–d) TEM of Co–S/G-3. (e) SAED pattern in panel c. (f and g) TEM of Co–S/G-2. Boundaries of the layered structure of the Co_3O_4 sheets in the composite are marked by arrows in (f). (h) XRD patterns of Co–P/G, Co–S-G-2 and Co–S/G-3. (i) High-resolution O 1s XPS spectra of Co–S/G-3 and Co–P/G. (j) High-resolution O 1s XPS of spectra of G and T–Co-S. The red arrows in panels a–g designate the interface between Co_3O_4 nanosheets and the graphene sheets.

and 513 cm^{-1} can be assigned to the F_{2g} modes of Co_3O_4, while the peak at 693 cm^{-1} can be assigned to A_{1g} mode.[26] These peaks were only observed on Co–P/G, suggesting that most Co_3O_4 nanoparticles are present on the graphene surface, in agreement with the XRD analysis (Figure 3h).

The XPS survey spectra reveal the presence of C 1s, O 1s, N 1s and Co 2p with no other impurities (Figure S7). The presence of Co_3O_4 nanosheets in Co–S/G-3 did not prevent nitrogen species incorporating into the graphene sheets, but rather facilitated its process (Figure S8). The measurements reveal that Co takes atomic percentage of 0.93, 1.38, 1.96, and 1.50 respectively in Co–S/G-3, Co–S/G-2, Co–S/G-1, and Co–P/G (Table S2). The higher Co content in Co–P/G than Co–S/G-3 with similar loading might suggests that most Co_3O_4 particles anchor into the surface of graphene sheet for Co–P/G, corresponding to the XRD and TEM analyses (Figures 3h and S9). Figure 3i,j show high-resolution O 1s XPS spectra of the composites, which can be deconvoluted into five peaks. The peak observed for Co–S/G-3 at 529.3 eV corresponds to oxygen from cobalt oxide,[27] consistent with the O 1s of Co_3O_4 sheets (Figure 3j). In Figure 3i, peaks observed at 530.6, 531.8, and 533.9 eV can be respectively assigned to the oxygen from the hydroxide (OH) ions, C═O groups and C–O–C groups (epoxide).[28] Peaks noticed at 533.6 and 533.9 eV on Co–P/G (20.8%) and Co–S/G-3 (7.5%) assigned to C–O–C groups (epoxide) are significantly lower in the composites as compared to the reduced graphene oxide (76.0%) (Figure 3j), suggesting a possible ring-opening reaction of the epoxy groups[29] with cobalt ions forming a C–O–Co linkage. The peaks noticed at 532.8 and 532.5 eV on Co–S/G-3 (36.5%) and Co–P/G (15.1%) can be assigned to the possible formation of the C–O–Co bond. There are more C–O–Co linkages for Co–S/G-3 than for Co–P/G, suggesting a stronger interfacial interaction between the Co_3O_4 nanosheets and the graphene.

Electrochemically Measured ORR Actvity. The electrocatalytic activities of Co–S/G-3, Co–S/G-2 and Co–S/G-1 for oxygen reduction reaction (ORR) were first investigated by cyclic voltammetry (CV) in 0.1 M KOH on a glassy carbon electrode in the presence of oxygen (O_2 bubbling) at room temperature with the same mass loading of ~0.08 mg cm^{-2} (Figures S10 and S11). As a benchmark, our composites performance was compared with a state-of-the-art commercial Pt/C (20% Pt on Vulcan XC-72, Premetek) under the same

DOI: 10.1021/acsami.5b06063
ACS Appl. Mater. Interfaces 2015, 7, 21373–21380

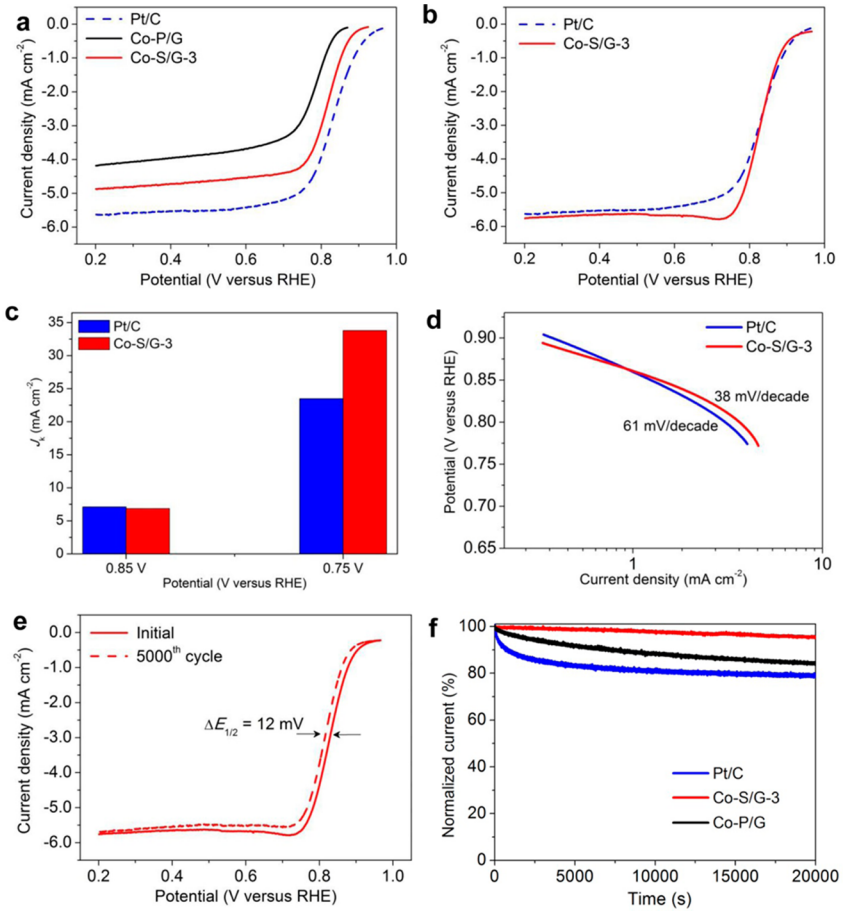

Figure 4. Electrochemical evaluation of catalysts. (a) Linear sweep voltammograms (LSVs) of Co−S/G-3, Co−P/G, and Pt/C at 1600 rpm in O_2-saturated 0.1 M KOH (scan rate: 10 mVs^{-1}). (b) LSVs of Co−S/G-3 and Pt/C at 1600 rpm. (c) Electrochemical activity given as the kinetic limiting current (J_k) at 0.75 and 0.85 V (vs RHE) for Co−S/G-3 and Pt/C. (d) Tafel plots of Co−S/G-3 and Pt/C. (e) LSVs of Co−S/G-3 measured during cycling durability in O_2-saturated (5000 cycles; potential range 0.6−1.0 V (vs RHE) at 50 mV/s). (f) Chronoamperometric responses of Co−S/G-3, Co−P/G, and Pt/C in O_2-saturated 0.1 M KOH.

condition with a Pt loading of 32 μg_{Pt} cm^{-2}.[7,8] The Co−S/G composites exhibit far more positive ORR peak potentials than Co−P/G, with the highest activity obtained for Co−S/G-3 (~0.805 V vs the reversible hydrogen electrode (RHE)). The ORR peak potential for Co−S/G-3 is ~39 mV more positive than Co−P/G and being only ~6 mV lower than the Pt/C. The electrocatalytic activity of Co−S/G-3 is further confirmed by recording the linear sweep voltammograms on a rotating-disk electrode (RDE) with the catalyst at a loading of ~0.08 mg cm^{-2}. Co−S/G-3 exhibits a half-wave potential ($E_{1/2}$) and an ORR onset potential of ~0.82 and 0.89 V, respectively (Figure 4a). The $E_{1/2}$ value of Co−S/G-3 is much higher than those of Co−S/G-1, Co−S/G-2, and Co−P/G (Figure S12). We can confirm that the $E_{1/2}$ value for the Pt/C (20% Pt on Vulcan XC-72) is ~0.833 V (Figure 4a), which is consistent with the literatures.[4,7,8,30−32]

Increasing the catalyst loading from ~0.08 to ~0.32 mg cm^{-2} shows the superior ORR activity of Co−S/G-3, as demonstrated by an $E_{1/2}$ value of ~0.832 V, which is comparable to the commercial Pt/C (Figure 4b). Impressively, a much higher current density of ~5.77 mA cm^{-2} was observed on Co−S/G-3 (Figure 4b), this value exceeded those of commercial Pt/C at both low and high overpotentials, implying that the electrode architecture of Co−S/G-3 is more effective in facilitating oxygen transport to the active sites for ORR than Pt/C (Figure 4b). This current density also represents the highest value of all nonprecious metal electrocatalysts and most Pt-based electrocatalysts (Table S3); and it is ~14 and ~19% higher than the highly active Co_3O_4 nanoparticles/nitrogen-doped graphene hybrids[4] and carbon nanotube/nanoparticle composite (N−Fe−CNT/CNP),[3] respectively (Table S3). Also, Co−S/G-3 and the commercial Pt/C exhibit comparable ORR onset potentials of ~0.930 and ~0.933 V, respectively (Figure 4b). We also confirm that the ORR activity of Co−S/G-3 can be further improved by increasing the catalyst loading to 0.64 mg cm^{-2}; this loading corresponds to current density of ~6.57 mA cm^{-2}, which is ~24 and 15% higher than the Co_3O_4 nanoparticles/nitrogen-doped graphene hybrids[4] and the state-of-the-art commercial Pt/C (Figure S13 and Table S3). Both the half-wave ($E_{1/2}$) and onset potential of Co−S/G-3 are more positive than most of the reported results for nonprecious metal electrocatalysts (Table S4), indicating that our material has very high electrocatalytic activity toward ORR in alkaline medium. The outstanding ORR activity of Co−S/G-3 was further quantitatively evaluated in terms of kinetic limiting current (J_k) on the basis of RDE measurements (Figure 4c). Remarkably, the J_k value of Co−S/G-3 exceeds that of state-of-the-art commercial Pt/C at 0.75 V vs RHE, and at 0.85 V both are comparable (~7 mA cm^{-2}).

DOI: 10.1021/acsami.5b06063
ACS Appl. Mater. Interfaces 2015, 7, 21373−21380

The excellent ORR activity of Co−S/G-3 is also reflected by its low Tafel slope of diffusion-corrected kinetic current density, which is ∼38 mV decade^{-1} at low overpotential (Figure 4d), equivalent to the lowest value reported on nonprecious metal electrocatalyst[4,18] and much lower than that of Pt/C (61 mV decade^{-1}).[33] The low Tafel slope of Co−S/G-3 indicates that the protonation of the adsorbed O^{2-} ions on the active sites is the rate limiting step.[4,18] It is well-known that the number of electrons (n) involved in ORR is vital to the catalyst performance. The reaction kinetics and number of electrons transferred per oxygen molecule on the samples were evaluated by conducting RDE measurements at different rotating speeds from 400 to 2500 rpm (Figure S14a,b). The electron transfer number (n) can be calculated based on the Koutecky−Levich (K−L) equation. The n value was calculated to be ∼4.0 at 0.40−0.70 V for Co−S/G-3 from the K−L plot slopes, suggesting a four-electron (4e) oxygen reduction process, which is similar to the commercial Pt/C (n ∼ 4.0 for Pt/C, Figure S14c,d). Rotating ring-disk electrode measurements (RRDE) were performed to verify the ORR catalytic pathways catalyzed by Co−S/G-3.[34] The measured peroxide yield is below 6% at all potentials, giving an average electron transfer number (n) of ∼3.9 (Figure S15). This is consistent with the result obatined from the K-L plots based on the RDE measurements (Figure S14), confirming that Co−S/G-3 favors the 4e process for ORR.

We investigated the electrochemical durability of the Co−S/G-3 by using the U.S. Department of Energy's accelerated durability test protocol by cycling the potential between 0.6 V and 1.0 (vs RHE) in O_2-staurated 0.1 M KOH at 50 mV/s.[35] As shown in Figure 3e, the half-wave potential ($E_{1/2}$) of Co−S/G-3 shows a small negative shift of ∼12 mV after 5000 cycles, which is far better than most nonprecious metal electrocatalysts,[35,36] while ∼17 mV loss of $E_{1/2}$ was observed for commercial Pt/C under the same conditions (Figure S16). Chronoamperometric testing confirms very good stability of the Co−S/G-3 with little decay in ORR activity over 20 000 s of continuous operation (Figure 4f). In contrast, the Pt/C and Co−P/G respectively suffered an activity loss of nearly 21 and 16%. The observed enhanced stability/durability of Co−S/G-3 as compared with the Pt/C and the Co−P/G can be attributed to the morphological architecture of Co_3O_4 nanosheets which facilitates strong interaction with the graphene sheet.

DFT Prediction of the Enhance Electrocatalytic Performance of Co−S/G-3. We conducted density funtional theory (DFT) calculations to unveil the origin of the highly enhanced ORR activity and excellent durability of the Co−S/G-3. Because Co_3O_4 (110) surface represents the dominant facets of the nanosheets in the experiment, a single-crystal Co_3O_4 (110) surface was first constructed. It is generally known that Co_3O_4 (110) can terminate in two ways: type-A surface where all O atoms are 3-fold-coordinate and type-B surface where half of oxygen atoms are 2-fold-coordinate.[37] The type B surface has a lower surface energy, especially in oxygen-rich conditions[38] and so the type-B Co_3O_4 (110) surface is used in our computational model. A single graphene layer comprising 40 carbon atoms was used to match a Co_3O_4 (110) layer containing 40 Co and 56 O atoms. Figures 5a and S17 show the side view and top view of the fully relaxed Co_3O_4 nanosheet/graphene and Co_3O_4 nanosheet/N-doped graphene geometries. It can be clearly seen from the optimized structures that the graphene sheet bends obviously on the Co_3O_4 (110) surface due to the strong electron coupling at the interface. The

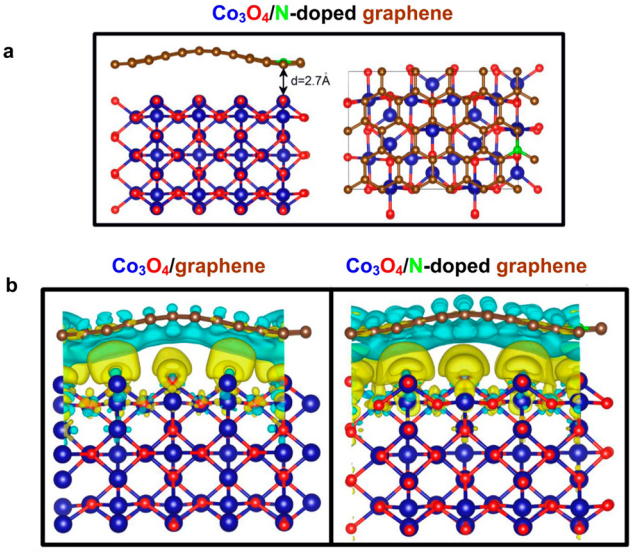

Figure 5. DFT calculation studies of Co−S/G-3. (a, left) The side and (right) top views of the optimized Co_3O_4 nanosheet/nitrogen-doped graphene composite (Co−S/G-3) interface. (b) The side view of 3D charge density difference plot for the interface between (left) a graphene sheet and a Co_3O_4 layer and a (right) N-doped graphene sheet and a Co_3O_4 layer. Yellow and cyan iso-surfaces represent charge accumulation and depletion in the 3D space with an iso-surface value of 0.004 e/Å^3. Brown, blue, red, and green balls represent C, Co, O, and N atoms, respectively.

shortest equilibrium distances between the graphene layer and the Co_3O_4 nanosheet are calculated to be 2.6 and 2.7 Å for Co_3O_4 nanosheet/graphene and Co_3O_4 nanosheet/N-doped graphene, respectively; these two composites correspond to high interface binding energy values −2.00 and −2.56 eV, confirming excellent stability.

To characterize the electron coupling at the Co_3O_4 nanosheet/graphene interface, three-dimensional charge density difference plots were calculated by subtracting electronic charge of Co_3O_4 nanosheet/graphene from separate graphene and Co_3O_4 layer as shown in Figure 5b. Clearly, there is significant charge transfer from graphene to the Co_3O_4 (110) top surface in the ground electronic state. The charge transfer could significantly improve the electron transport through the whole structure and consequently the ORR activity. Furthermore, the N-doped graphene will become hole-doped due to the charge transfer, leading to the structural rippling on the Co_3O_4 (110) surface and therefore the highly improved ORR electrocatalytic activity of Co−S/G-3.

CONCLUSIONS

For the first time, we developed a Co_3O_4 nanosheet-graphene composite (Co−S/G-3) that was used as an ORR electrocatalyst exhibiting superior activity and stability to the state-of-the-art commercial Pt/C in alkaline solution. Its electrocatalytic activity exceeds those of other nonprecious metal electrocatalysts, including the recently published Co_3O_4 nanoparticles/nitrogen-doped graphene hybrids[4] and the carbon nanotube/nanoparticle composite (N−Fe−CNT/CNP).[3] Experimental observations in combination with density functional theory (DFT) calculations revealed that the superior electrocatalytic activity of Co−S/G-3 originated from the enhanced electron transport through the whole composite structure due to the significant charge transfer from graphene to Co_3O_4

DOI: 10.1021/acsami.5b06063
ACS Appl. Mater. Interfaces 2015, 7, 21373−21380

nanosheets. The Co−S/G-3 displayed an excellent accelerated durability test (5000 cycles) as compared with commercial Pt/C in alkaline solution. Theoretical calculations confirmed that a strong interaction was generated between the Co_3O_4 nanosheets and the graphene with a high interfacial binding energy, indicating very high stability. These findings will facilitate the development of new families of high-performance ORR electrocatalysts based on a sheet-on-sheet heterostructure.

■ ASSOCIATED CONTENT

Supporting Information

The Supporting Information is available free of charge on the ACS Publications website at DOI: 10.1021/acsami.5b06063.

Nitrogen adsorption/desorption measurements, pore size distribution, XRD patterns, SEM and HRTEM images, Raman spectra, XPS characterizations, CV curves and linear sweep voltammograms, percentage of peroxide and electron transfer number data, DFT calculation studies, characteristics of electrocatalysts, XPS data, summary of reported current densities, summary of reported half-wave potential, and summary of reported kinetic limiting current. (PDF)

■ AUTHOR INFORMATION

Corresponding Author

*Fax: +61 73365 4199. E-mail: z.zhu@uq.edu.au.

Notes

The authors declare no competing financial interest.

■ ACKNOWLEDGMENTS

The authors acknowledge the facilities and the scientific and technical assistance of the Australian Microscopy and Microanalysis Research Facility at the Centre for Microscopy and Microanalysis, at The University of Queensland. The first author also acknowledges the support from International Postgraduate Research Scholarship (IPRS) and UQ Centennial Scholarship (UQ Cent).

■ REFERENCES

(1) Chu, S.; Majumdar, A. Opportunities and Challenges for a Sustainable Energy Future. *Nature* **2012**, *488*, 294−303.

(2) Vayssilov, G. N.; Lykhach, Y.; Migani, A.; Staudt, T.; Petrova, G. P.; Tsud, N.; Skala, T.; Bruix, A.; Illas, F.; Prince, K. C.; Matolin, V.; Neyman, K. M.; Libuda, J. Support Nanostructure Boosts Oxygen Transfer to Catalytically Active Platinum Nanoparticles. *Nat. Mater.* **2011**, *10*, 310−315.

(3) Chung, H. T.; Won, J. H.; Zelenay, P. Active and Stable Carbon Nanotube/Nanoparticle Composite Electrocatalyst for Oxygen Reduction. *Nat. Commun.* **2013**, *4*, 1922−1926.

(4) Liang, Y.; Li, Y.; Wang, H.; Zhou, J.; Wang, J.; Regier, T.; Dai, H. Co_3O_4 Nanocrystals on Graphene as a Synergistic Catalyst for Oxygen Reduction Reaction. *Nat. Mater.* **2011**, *10*, 780−786.

(5) Keith, J. A.; Jacob, T. Theoretical Studies of Potential-Dependent and Competing Mechanisms of the Electrocatalytic Oxygen Reduction Reaction on Pt(111). *Angew. Chem., Int. Ed.* **2010**, *49*, 9521−9525.

(6) Guo, S.; Zhang, S.; Sun, S. Tuning Nanoparticle Catalysts for the Oxygen Reduction Reaction. *Angew. Chem., Int. Ed.* **2013**, *52*, 8526−8544.

(7) Liang, J.; Jiao, Y.; Jaroniec, M.; Qiao, S. Z. Sulfur and Nitrogen Dual-Doped Mesoporous Electrocatalyst for Oxygen Reduction with Synergistically Enhance Performance. *Angew. Chem., Int. Ed.* **2012**, *51*, 11496−11500.

(8) He, W.; Jiang, C.; Wang, J.; Lu, L. High-Rate Oxygen Electroreduction over Graphitic-N species Exposed on 3D Hierarchically Porous Nitrogen-Doped Carbons. *Angew. Chem., Int. Ed.* **2014**, *53*, 9503−9507.

(9) Maldonado, S.; Stevenson, K. J. Influence of Nitrogen Doping on Oxygen Electrocatalysts at Carbon Nanofiber Electrodes. *J. Phys. Chem. B* **2005**, *109*, 4707−4716.

(10) Novoselov, K. S.; Geim, A. K.; Morozov, S. V.; Jiang, D.; Zhang, Y.; Dubonos, S. V.; Grigorieva, I. V.; Firsov, A. A. Electric Field Effect in Atomically Thin Carbon Films. *Science* **2004**, *306*, 666−669.

(11) Odedairo, T.; Ma, J.; Gu, Y.; Chen, J.; Zhao, X. S.; Zhu, Z. One-Pot Synthesis of Carbon-Nanotube-Graphene Hybrids via Syngas Production. *J. Mater. Chem. A* **2014**, *2*, 1418−1428.

(12) Li, W. Y.; Xu, L. N.; Chen, J. Co_3O_4 Nanomaterials in Lithium-Ion Batteries and Gas Sensors. *Adv. Funct. Mater.* **2005**, *15*, 851−857.

(13) Feng, J.; Zeng, H. C. Size-Controlled Growth of Co_3O_4 Nanocubes. *Chem. Mater.* **2003**, *15*, 2829−2835.

(14) Lou, X. W.; Deng, D.; Lee, J. Y.; Feng, J.; Archer, L. A. Self-Supported Formation of Needlelike Co_3O_4 Nanotubes and Their Application as Lithium-Ion Battery Electrodes. *Adv. Mater.* **2008**, *20*, 258−262.

(15) Ma, J.; Meng, Q.; Michelmore, A.; Kawashima, N.; Izzuddin, Z.; Bengtsson, C.; Kuan, H. C. Covalently Bonded Interfaces for Polymer/Graphene Composites. *J. Mater. Chem. A* **2013**, *1*, 4255−4264.

(16) Ma, J.; Meng, Q.; Zaman, I.; Zhu, S.; Michelmore, A.; Kawashima, N.; Wang, C. H.; Kuan, H. C. Development of Polymer Composites Using Modified, High-Structural Integrity Graphene Platelets. *Compos. Sci. Technol.* **2014**, *91*, 82−90.

(17) Li, F.; Lu, Y.; Liu, L.; Zhang, L.; Dai, J.; Ma, J. Relations Between Carbon Nanotubes Length and Their Composites Mechanical and Functional Performance. *Polymer* **2013**, *54*, 2158−2165.

(18) Liang, Y.; Wang, H.; Zhou, J.; Li, Y.; Wang, J.; Regier, T.; Dai, H. Covalent Hybrid of Spinel Manganese-Cobalt Oxide and Graphene as Advanced Oxygen Reduction Electrocatalysts. *J. Am. Chem. Soc.* **2012**, *134*, 3517−3523.

(19) Zheng, Y.; Jiao, Y.; Jaroniec, M.; Jin, Y.; Qiao, S. Z. Nanostructured Metal-Free Electrochemical Catalysts for Highly Efficient Oxygen Reduction. *Small* **2012**, *8*, 3550−3566.

(20) Hunter, D.; Osborn, W.; Wang, K.; Kazantseva, N.; Hattrick-Simpers, J.; Suchoski, R.; Takahashi, R.; Young, M.; Mehta, A.; Bendersky, L.; Lofland, S.; Wuttig, M.; Takeuchi, I. Gaint Magnetostriction in Anneled $Co_{1-x}Fe_x$ Thin-Films. *Nat. Commun.* **2011**, *2*, 518−524.

(21) Sun, J.; Zheng, S.; Zhang, K.; Song, D.; Liu; Sun, X.; Chen, J. The Crystal Plane Effect of CoFe Nanocrystals on Fischer−Tropsch Synthesis. *J. Mater. Chem. A* **2014**, *2*, 13116−13122.

(22) Araby, S.; Zhang, L.; Kuan, H. C.; Dai, J. B.; Majewski, P.; Ma, J. A Novel Approach to Electrically and Thermally Conductive Elastomers Using Graphene. *Polymer* **2013**, *54*, 3663−3670.

(23) Araby, S.; Meng, Q.; Zhang, L.; Kang, H.; Majewski, P.; Tang, Y.; Ma, J. Electrically and Thermally Conductive Elastomer/Graphene Nanocomposites by Solution Mixing. *Polymer* **2014**, *55*, 201−210.

(24) Nam, K. M.; Shim, J. H.; Han, D. W.; Kwon, H. S.; Kang, Y. M.; Li, Y.; Song, H.; Seo, W. S.; Park, J. T. Syntheses and Characterization of Wurtzite CoO, Rocksalt CoO, and Spinel Co_3O_4 Nanocrystals: Their Interconversion and Tuning of Phase and Morphology. *Chem. Mater.* **2010**, *22*, 4446−4454.

(25) Zhu, Y. W.; Murali, S.; Stoller, M. D.; Ganesh, K. J.; Cai, W.; Ferreira, P. J.; Pirkle, A.; Wallace, R. M.; Cychosz, K. A.; Thommes, M.; Su, D.; Stach, E. A.; Ruoff, R. S. Carbon-Based Supercapacitors Produced by Activation of Graphene. *Science* **2011**, *332*, 1537−1541.

(26) Dong, X. C.; Xu, H.; Wang, X. W.; Huang, Y. X.; Chan-Park, M. B.; Zhang, H.; Wang, L. H.; Huang, W.; Chen, P. 3D Graphene-Cobalt Oxide Electrode for High-Performance Supercapacitor and Enzymeless Glucose Detection. *ACS Nano* **2012**, *6*, 3206−3213.

(27) Yang, J.; Liu, H.; Martens, W. N.; Frost, R. L. Synthesis and Characterization of Cobalt Hydroxide, Cobalt Oxyhydroxide, and Cobalt Oxide Nanodiscs. *J. Phys. Chem. C* **2010**, *114*, 111−119.

DOI: 10.1021/acsami.5b06063
ACS Appl. Mater. Interfaces 2015, 7, 21373−21380

(28) Gardner, S. D.; Singamsetty, C. S. K.; Booth, G. L.; He, G. R.; Pittman, C. U. Surface Characterization of Carbon Fibers Using Angle-Resolved XPS and ISS. *Carbon* **1995**, *33*, 587−595.
(29) Pei, S.; Zhao, J.; Du, J.; Ren, W.; Cheng, H. M. Direct Reduction of Graphene Oxide Films into Highly Conductive and Flexible Graphene Films by Hydrohalic Acids. *Carbon* **2010**, *48*, 4466−4474.
(30) Li, Y.; Zhang, H.; Wang, Y.; Liu, P.; Yang, H.; Yao, X.; Wang, D.; Tang, Z.; Zhao, H. A Self-Sponsored Doping Approach for Controllable Synthesis of S and N Co-doped Trimodal-Porous Structured Graphitic Carbon Electrocatalysts. *Energy Environ. Sci.* **2014**, *7*, 3720−3726.
(31) Wang, D.; Chen, X.; Evans, D. G.; Yang, W. Well-Dispersed Co_3O_4/Co_2MnO_4 Nanocomposites as a Synergistic Bifunctional Catalyst for Oxygen Reduction and Oxygen Evolution Reactions. *Nanoscale* **2013**, *5*, 5312−5315.
(32) Zheng, Y.; Jiao, Y.; Ge, L.; Jaroniec, M.; Qiao, S. Z. Two-Step Boron and Nitrogen Doping in Graphene for Enhanced Synergistic Catalysis. *Angew. Chem.* **2013**, *125*, 3192−3198.
(33) Suntivich, J.; Gasteiger, H. A.; Yabuuchi, N.; Shao-Horn, Y. Electrocatalytic Measurement Methodology of Oxide Catalysts Using a Thin-Film Rotating Disk Electrode. *J. Electrochem. Soc.* **2010**, *157*, B1263−B1268.
(34) Odedairo, T.; Ma, J.; Gu, Y.; Zhou, W.; Jin, J.; Zhao, X. S.; Zhu, Z. A New Approach to Nanoporous Graphene Sheets via Rapid Microwave-Induced Plasma for Energy Applications. *Nanotechnology* **2014**, *25*, 495604−495613.
(35) Wu, G.; More, K. L.; Johnston, C. M.; Zelenay, P. High-Performance Electrocatalysts for Oxygen Reduction derived from Polyaniline, Iron, and Cobalt. *Science* **2011**, *332*, 443−447.
(36) Li, Y.; Zhou, W.; Wang, H.; Xie, L.; Liang, Y.; Wei, F.; Idrobo, J. C.; Pennycook, S. J.; Dai, H. An Oxygen Reduction Electrocatalyst Based on Carbon Nanotube-Graphene Complexes. *Nat. Nanotechnol.* **2012**, *7*, 394−400.
(37) Jiang, D.; Dai, S. The Role of Low-Coordinate Oxygen on Co_3O_4 (110) in Catalytic CO Oxidation. *Phys. Chem. Chem. Phys.* **2011**, *13*, 978−984.
(38) Xu, X. L.; Chen, Z. H.; Li, Y.; Chen, W. K.; Li, J. Q. Bulk and Surface Properties of Spinel Co_3O_4 by Density Functional Calculations. *Surf. Sci.* **2009**, *603*, 653−658.

DOI: 10.1021/acsami.5b06063
ACS Appl. Mater. Interfaces 2015, 7, 21373−21380